Optical transmittance of 2D crystals and ultra thin black phosphorus

Rebekah Chua

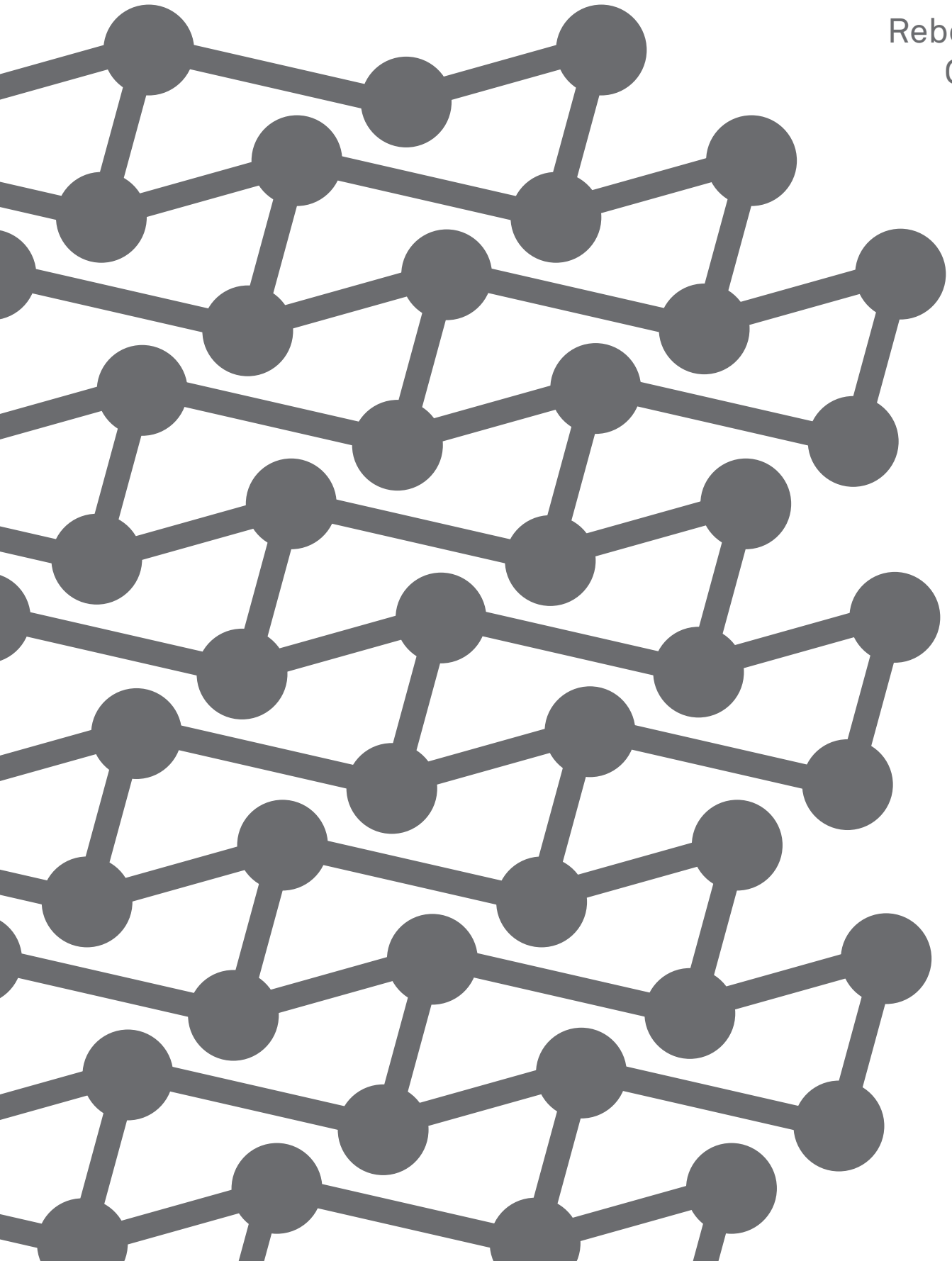

Optical transmittance of 2D crystals and ultra thin black phosphorus

Rebekah Chua

Abstract

Nearly all bulk semiconductor crystals are known to be opaque to light in the visible range of the electromagnetic spectrum. However, research in the field of two-dimensional materials, during the past decade, has enabled the preparation of crystalline semiconducting films with atomic thickness of below one nanometer. The ultra thin nature of two-dimensional crystals means that their thickness is well below the absorption depth for light, allows the study of their optical properties using transmission spectroscopy and enables their application in next-generation transparent electronics. In this report, a systematic and comparative study is done on the experimentally measured optical transmittance of exfoliated 2D crystals and their heterostructures. When comparing the studied materials of similar thickness, boron nitride exhibits the highest optical transmittance while molebdenum disulfide is the most opaque. This is explained by the band structures and the corresponding value for the energy gap. Due to the weak interaction between the individual layers in heterostructures, the optical transmittance of the heterostructure is found to be similar to the transmittance of the individual layers. In the optical transmittance study of ultra thin black phosphorus, it was found that the anisotropy of the crystal structure leads to a polarization-dependent transmittance, with a difference of up to 3.7% at different relative angles. This optical anisotropic feature of black phosphorus provides a direction-dependent control over its opacity which could be useful in the design of novel optoelectronic devices.

Contents

Introduction

Ever since the discovery of graphene and its electric field tunable electronic properties by Novoselov et al.[1], extensive research has been carried out on two dimensional (2D) materials. When reduced to two dimensions, the crystals exhibit different properties from those found in their bulk form. For example, electrons in graphene obey a linear dispersion relation and behave like massless relativistic particles, which is different than the finite effective mass for the electrons in bulk graphite[2,3]. Also, the transition metal dichalcogenide (TMD) monolayers exhibit a direct band gap at the K point, while the bulk crystals are indirect band gap semiconductors[4-7]. This change in the band structure is usually accompanied with an increase in band gap value when going from bulk to monolayer form. The reason for these distinctive changes when transitioning from three to two dimensions is the quantum confinement effect[8,9]. It is observed when the thickness of the crystal becomes comparable to the wavelength of the electron. When the motion of the electrons is confined due to geometrical constraints, its energy is restricted to specific (discrete) energy levels. As the thickness of the crystal decreases, the energy levels become discrete, which widens up the band gap[10]. The tunable band gap with varying thickness of 2D materials could lead to a wide variety of applications in electronics and opto-electronics. The 2D materials are also seen to maintain their electrical and optical properties while bent, stretched and rolled which makes them suitable candidates for flexible electronics[8].

Currently, the most well studied 2D materials are graphene, boron nitride (BN), and TMDs, in particular MoS_2 and WS_2. These 2D crystals exhibit diverse electronic properties and they can be metallic, insulating, or semiconducting. Graphene, a monolayer of graphite, is a semimetal with zero gap and is well known for its high electron mobility[11]. BN is an insulator with a large band gap of ~6.5 eV[12] and has a high optical transparency. The TMDs are denoted by MX_2, with M a transition metal atom (Mo, W, etc.) and X a chalcogen atom (S, Se, or Te). In the bulk form, the TMDs have indirect band gaps in the near infrared frequencies, such as 1.3 eV for bulk MoS_2[5] and 1.4 eV for bulk WS_2[13]. When thinned down to a monolayer, MoS_2 and WS_2 have direct bandgaps of 1.8 eV and 2.1 eV respectively[5,13].

In 2014, phosphorene, a monolayer of black phosphorus (bP), was made experimentally possible by mechanical exfoliation of bP and it was found to be a very promising material due to its high mobility[14-16] and finite band gap. bP is a layered semiconductor that has a direct band gap of 0.3 eV in the bulk form and 2 eV in the single layer form of phosphorene[17,18]. This makes it possible to bridge the band gap energy rang between graphene, a zero gap material, and TMDs, with a band gap of usually 1.3 - 1.4 eV in the bulk form. A significant property of bP is its highly anisotropic in-plane crystal structure, due to the sp^3 hybridization of the P bonds[19-21]. This leads to anisotropic optical, electrical, and mechanical properties[20,22-24] which has spurred the research on bP-based electronic and optical devices. The anisotropy of the optical properties of bP could be useful for next generation optoelectronic devices, because it provides an additional design parameter.

A noteworthy feature of the 2D crystals is their high optical transparency when the materials are thinned down to a monolayer. The bulk materials such as graphite, bulk MoS_2, WS_2, or bP are known to be opaque, but are experimentally seen to increase in transparency with decreasing number of layers. The low opacity of the thin layers enables optical transmittance measurement in the visible light range, which was previously not possible with the bulk materials. The study of the optical transmittance is advantageous for novel transparent electronics applications which require materials of high optical transparency with high electrical conductivity. As of yet, only the optical transmittance of graphene has been properly studied[25]. A systematic study and comparison of the optical of 2D materials, particularly their optical transmittance, is therefore essential before their potential application in transparent electronics.

This project attempts to characterise the optical properties of various mechanically exfoliated 2D crystals, especially ultra thin black phosphorus, by measuring their optical transmittance in the visible light spectrum on a transparent substrate. This experiment uses transmission spectroscopy, which is a direct method to measure the optical transmittance of 2D materials. The experimental set up is able to measure over a very small area, hence requiring only small-sized exfoliated crystals. This report is organized as follows: A literature review of the recent research and published results is presented in the chapter “Current Research”. Next, the chapter “Experimental Methods” gives the details of the experimental methods used to fabricate, characterise, and measure the optical transmittance of the studied 2D crystals and heterostructures. The chapter “Results” presents the experimental findings from the optical transmittance measurements. The physics behind the measured results is then discussed in the chapter “Discussion”. Finally, the conclusion of this project and its future outlook is discussed in the chapter “Conclusion & Outlook”.

Current Research

This chapter summarizes the published results on the optical transmittance of 2D materials. Each section of this chapter provides a short literature review for each crystal studied in this project.

Graphene

Nair et al.[26] was the first to study the optical transmittance of graphene. It was found that graphene has an optical opacity of 2.3%, which increases by another 2.3% with every additional layer. The exfoliated graphene samples were attached to a support structure of a perforated 20 µm thick copper-gold film fabricated using photolithography. The films had 9 small apertures with diameters of 20, 30 and 50 µm. The optical transmittance was measured by shining a light source through the aperture and detecting the light intensity with a spectrometer. This measurements were taken with respect to either an empty space or, as a double check, another aperture of the same size but without graphene. The optical transmittance, T, of graphene was found to be independent of wavelength in the visible spectrum, and follows the relation:

$$(1-T) \approx \pi\alpha$$

where $\alpha = {e^2}/{\hbar c} \approx {1}/{137}$ is the fine struture constant. Subsequently, Falkovsky[26] also studied the reflectance and transmittance of graphene monolayer and multilayers. The dynamic conductivity was calculated theoretically at different frequency, temperature, and chemical potential. Again, it was also shown that the transmittance of graphene in the visible range is independent of frequency and is defined by the fine structure constant. It was also found that the reflectance of graphene is determined by the intraband Drude-Boltzmann conductivity in the infra-red region and by the interband absorption for higher frequencies.

Hexagonal Boron Nitride

The optical absorption of hexagonal BN thin films was studied by Zunger, Katzir, and Halperin[27]. The BN sample was grown on a quartz substrate using chemical vapor deposition (CVD), and measured to be 68 nm in thickness. Using a spec- trophotometer, the absorption coefficient was measured in the near-UV range (195 - 320 nm). An absorption peak was observed at 6.2 eV, followed by a sharp decrease in absorption coefficient at lower energies due to the direct band gap.

Song et al.[28] also measured the optical absorbance of few layer BN. The CVD-grown BN sample was measured to be ~1.3 nm thick and a spectrophotometer was used to measure the absorbance in the UV-vis region (200 - 900 nm). A sharp absorbance peak was observed at 203nm (6.1 eV), which is consistent with the results of the absorption coefficient of bulk BN presented by Zunger, Katzir, and Halperin[27]. In the range of 250 - 900 nm, the BN film was observed to transmit almost 99% of the incident light. The optical band gap was also measured to be 5.56 eV.

Transition Metal Dichalcogenides

Yu et al.[9] measured the dielectric function of MoS_2 films of different thickness and demonstrated the strong impact of excitonic effects on the dielectric functions for films thinner than 5 - 7 layers thick. The dielectric function does not have a consistent dependance on layer number, because it is observed to decrease with in- creasing layer number when the films are less than 5 - 7 layers thick, and then it starts to increase with layer number above that thickness. The MoS_2 films were grown using the CVD process on sapphire substrates and the dielectric function was measured using spectroscopic elipsometry. In the graph of dielectric function against photon excitation energy, there are three peaks observed which are due to excitonic transitions A, B, and C, labelled from low to high energies. The C exciton peak position was seen to evolve with the layer number and it is proposed that quantum confinement effects may be the reason.

Kumar, Verzhbitskiy and Eda[29] have studied the absorption of exfoliated monolayer MoS_2. The absorption spectrum was obtained by measuring the intensity of transmitted and reflected light in a transmission microscope set up. The strong optical absorption traits were attributed to be due to band nesting and corresponding divergence of the joint density of states, which is characteristic to 2D structures. They measured the wavelength-dependent absorption of monolayer MoS_2 in the visible light range and found that the A and B exciton peaks have 10% absorption while the C exciton peak has 30% absorption.

The dielectric function of various exfoliated monolayer TMDs were studied by Li et al.[30], which were MoS_2, $MoSe_2$, WS_2 and WSe_2. The dielectric function was obtained from the reflectance spectrum, which was measured using a broadband light source at room temperature. The imaginary part of the dielectric function was determined from the reflectance spectrum and was converted to the real part of the dielectric function through a Kramers-Kronig constrained analysis. The A, B and C exciton peaks were observed within the range of 1.5 eV (827 nm) $\leq$ E $\leq$ 3 eV (413 nm) in both the real and imaginary parts of the dielectric function. When compared with the dielectric function of the bulk materials, the peak positions and intensity changes, with a lower intensity of the exciton peaks for the TMDs.

Black Phosphorus

The optical transmittance of few layer exfoliated bP was studied by Castellanos-Gomez et al[31]. Using a microscope with an attached digital camera, the intensity of the red, green, and blue colour channels of the transmission mode optical image were measured with respect to the substrate to obtain a transmittance histogram. It was seen that the thinner bP samples have a higher optical transmittance of light. The integrated absorbance of the black phosphorus samples in the visible light spectrum was measured to be a multiple of 2.8%, so it was deduced that phosphorene has an absorbance of 2.8%.

In other works that presents the optical properties of bP, the optical absorption was shown to vary with light polarised along different angles along the bP crystal axis. It was measured to be 15% for light polarized along the x-axis of the bP crystal structure for a 40 nm bP sample, while it is 2% for light polarized along the y-axis[32].

Scope of this project

Despite some published results on the optical properties of 2D materials, there is still no systematic comparative study of their optical transmittance in the visible range. Furthermore, the values for the absorption and transmittance in the literature are often obtained using indirect measurements, such as reflectance spectroscopy or optical ellipsometry. Also, there is no systematic comparison of the optical transmittance with varying layer number and between different classes of 2D materials. As such, this project aims to directly measure the optical transmittance of various 2D crystals exfoliated on a transparent quartz substrate. The results of this project can give insights on the physics that determines (and limits) the optical transparency of 2D materials. This could have practical importance in evaluating the suitability of 2D crystals for next-generation transparent electronics.

Experimental Methods

This chapter discusses the experimental methods to fabricate, characterise, and measure the optical transmittance of graphene, BN, MoS_2, WS_2, bP, and MoS_2-WS_2 and MoS_2-BN heterostructures. All parts of this experiment was done in a class 1,000 cleanroom with controlled 50% relative humidity, except for exfoliation and encapulation of bP which were done in a glove box, molecular beam epitaxy which was done in ultra high vacuum condition at room temperature, and optical spectroscopy which was done in ambient conditions.

Exfoliation

The 2D crystals of interest are fabricated by mechanical exfoliation using blue Nitto tape and then exfoliated on transparent quartz slides of 10 x 10 x 0.5 mm that were purchased from Latech, as seen in Figure 1. In this experiment, all samples are exfoliated on quartz slides to allow optical transmission measurements. The types of crystals being exfoliated are graphene, BN, MoS_2, WS_2, and bP.

Graphene was exfoliated from a bulk highly oriented pyrolytic graphite (HOPG) crystal that was purchased from NGS Naturgraphit GmbH. MoS_2 crystals was exfoliated from bulk MoS_2 that was purchased from SPI Supplies. The WS_2 used were exfoliated from bulk crystals of 2H-WS_2 that were grown by the chemical-vapour transport method using iodine as the transport agent[33,34]. The hBN crystals were exfoliated from a bulk hBN single crystal grown by a Ba-BN solvent method[35]. Bulk bP crystals were purchased from HQ Graphene and exfoliated onto quartz slides in an Ar-filled glovebox with an O_2 and H_2O concentration of less than 2 p.p.m. No degradation of the bP crystals is observed in the Ar gas environment.

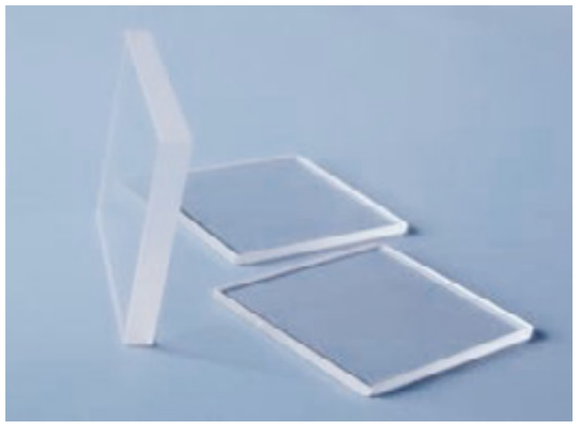

Figure 1 Quartz slides from Latech.

Transfer

Dry transfer is performed to form heterostructures[33,36] or to encapsulate bP[37]. Firstly, a crystal of interest is exfoliated onto a SiO_2/Si wafer coated with polymethylglutarimide (PMGI) and polymethylmethacrylate (PMMA) in a spin-coater (WBS-400BZ-6NPP), which serve as the release and support polymer layers, respectively. After identifying a suitable transfer sample with a microscope (Nikon Eclipse LV100D), the PMGI is developed and the transfer sample held by the PMMA polymer layer is placed on a transfer slide. To transfer on bP, the transfer slide is brought into the glovebox. The transfer is then completed by lowering the transfer sample onto another exfoliated 2D crystal on a quartz slide using a micromanipulator. After the transfer is complete, the support PMMA layer is removed in acetone.

Another form of encapsulation of few layer bP is to perform Molecular Beam Epitaxy (MBE) where magnesium oxide (MgO) of 10nm thickness is deposited on bP crystals exfoliated on quartz. The bP sample is transferred into the MBE system that is custom-made by Omicron through an Ar-filled glovebox to ensure that the O_2 and H_2O concentration is less than 2 p.p.m. After careful placement of the bP sample, the system is pumped to ultra-high vacuum conditions (10^{-8} Torr) at room temperature before the MBE process takes place at 1 Å/s.

	Wafer Grade
Material:	Quartz (SiO2 > 99.99%)
Material Grade:	JGS-1
Polishing:	Double-side epi-polished (Ra < 1 nm)
Transmittance: (Thickness 1 mm)	• > 90% at 260 - 2600 nm • > 80% at 210 - 260 nm • > 70% at 180 - 210 nm
Appearance:	Highly transparent quartz slides
Dimension:	10 x 10 x 0.5 mm
Temperature:	Can work at 1100 °C continuously
Comments:	Acid resistant except HF acid, excellent insulating behavior, long-lasting and environmental friendly

Table 1 Specifications of quartz slides from Latech.

Thickness determination

The exfoliated samples are characterised by their thickness or layer number. Each material has their own unique set of characterisation methods, which are noted in Figure 2. The characterisation methods are described in the following subsections.

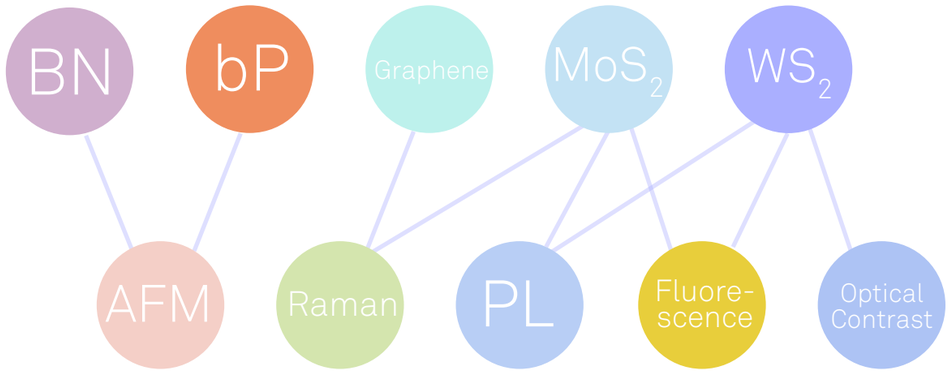

Figure 2 The studied 2D crystals and their respective characterisation method

Raman spectroscopy

Raman spectroscopy is used to determine the layer number of graphene and MoS_2 samples. It is performed using an Alpha 300 R in the backscattering configuration with a 532 nm laser excitation. The Raman spectrum of graphene has two distinct bands which are the G and 2D band, located at Raman shift positions of approximately 1580 cm^{-1} and 2700 cm^{-1} respectively. The intensity ratio I_{2D}/I_G of these bands for graphene is equals to 4. With these features identified, graphene is successfully characterised[33]. In the case of MoS_2, the relative distance between the E_{2g} and A_{1g} peaks inceases with increasing layer numbers[39], as seen in Figure 3 and Figure 4. As such, the layer number of MoS_2 is determined with Raman spectroscopy, up to several layers.

Atomic force microscopy

Atomic force microscopy (AFM) is performed to measure the thickness of BN and bP. The AFM scans were acquired using a Bruker Dimension FastScan microscope in tapping or contact mode. The thickness of the crystal is obtained by measuring the relative height of the sample with respect to the quartz background and appropriately flattening and manipulating the AFM scans using Gwyddion. A 1 x 1 µm image of the sample border on a quartz background is ideal for measuring the step height of the sample, as seen in Figure 6. A line is drawn across the border with a certain width to obtain an averaged step height profile, as seen in Figure 7. There will be a distinct step seen in the graph which represents the height. Precise measurement of the height is taken by averaging the values of the two plateaus and taking their difference.

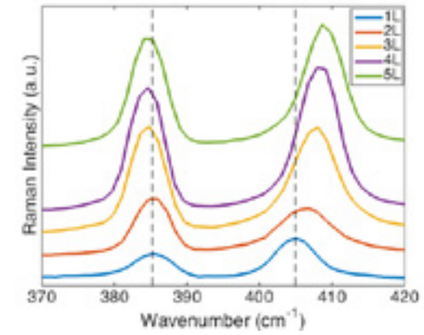

Figure 3 Measured Raman spectrum between the E_{2g} and A_{1g} peaks of 1 - 5 layers of MoS_2.

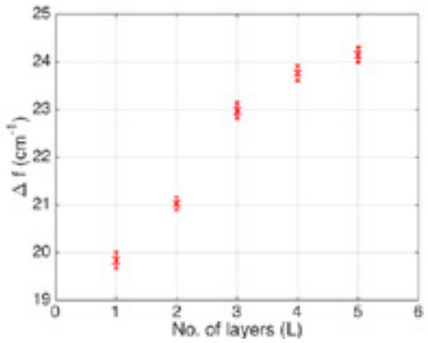

Figure 4 Wavenumber difference between the E_{2g} and A_{1g} peaks of 1 - 5 layers of MoS_2.

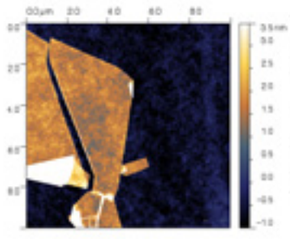

Figure 5 10x10 µm AFM scan of a BN sample. The red box shows the AFM image in Figure 6.

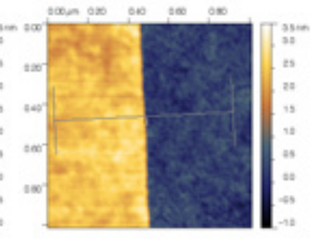

Figure 6 1x1 µm AFM scan of a BN sample, with a line drawn across to obtain the step height profile in Figure 7.

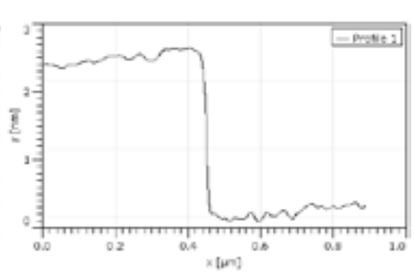

Figure 7 Step height profile of a BN sample from AFM measurement. The measured height on the BN flake is taken by averaging the values of the two plateaus and taking their difference. It gives a height of 2.37 nm.

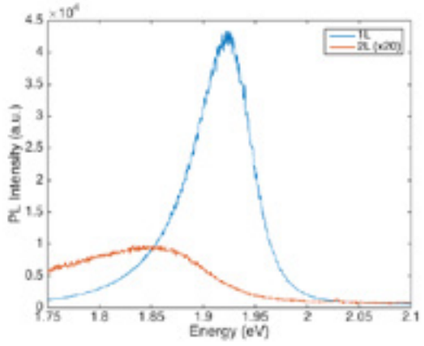

Figure 8 Measured photoluminescence spectrum of monolayer and bilayer WS_2 on a quartz substrate.

Photoluminescence Spectroscopy

Photoluminescence (PL) is used to determine monolayers of MoS_2 and WS_2. It is performed using a Alpha 300 R with a 532 nm laser excitation. In the PL experiment, the sample is excited by photons with an energy larger than the bandgap energy. Once the photons are absorbed, electrons and holes are formed in the conduction and valence bands, respectively. The excitations undergo energy and momentum relaxation towards the band gap minimum. Typical mechanisms are Coulomb scattering and the interaction with phonons. The electrons then recombine with holes which emits photons. This occurs in monolayers of TMDs due to the direct band gap of monolayers. In the case of bilayer and thicker samples, there would not be significant or any PL signal produced because of their indirect band gap. Photoexcitations alone would not be enough to excite electrons to the conduction band; phononic excitations are needed. As such, the PL signal in monolayer TMDs would be of much higher intensity as compared to those from thicker samples and it is a plausible way to distinguish monolayers from thicker samples[4,5]. A sample photoluminescence spectrum of monolayer and bilayer WS_2 is seen in Figure 8.

Fluorescence Spectroscopy

Fluorescence sepectroscopy is also used to determine monolayers of MoS_2 and WS_2. It is done by using a microscope (Nikon Eclipse LV100D) attached with a mercury lamp (Nikon Intensilight Epi-fluorescence Illuminator). Only monolayers of MoS_2 and WS_2 would produce fluorescence due to the direct band gap of the monolayers. Similar to the PL experiment, energy from the photons is enough to excite the electrons from the valence band to the conduction band, which would recombine with the hole produced in the valence band to produce fluorescence. Increasing number of layers of MoS_2 and WS_2 have indirect band gaps and require phononic excitations for electrons to jump from the valence band to conduction band. As such, bilayers and thicker samples do not produce fluorescence when shone under a fluorescence lamp. Fluorescence of monolayers is seen most clearly with the optical filters of 450 - 490 nm and 400 - 440 nm for MoS_2 and WS_2 respectively. A sample image of the fluorescence of exfoliated monolayer MoS_2 can be seen in Figure 10.

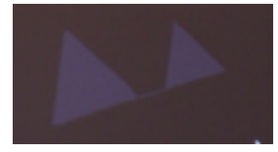

Figure 9 Optical image of exfoliated monolayer MoS_2.

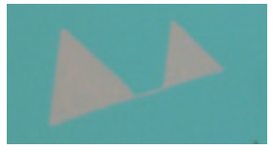

Figure 10 Fluorescence image of exfoliated monolayer MoS_2.

Optical Contrast

Optical contrast is used to identify the layer number of WS2. Following the concept of Hai Li, et al.[40], the optical contrast of WS_2 on quartz is seen to increase with increasing thickness when the contrast difference of red, green, and blue colour light of the sample is measured with respect to the optical contrast of the quartz background. This method is able to reliably determine the layer number of WS_2, up to a few layers. The graph of increasing contrast difference of blue light with increasing layer number is seen in Figure 11.

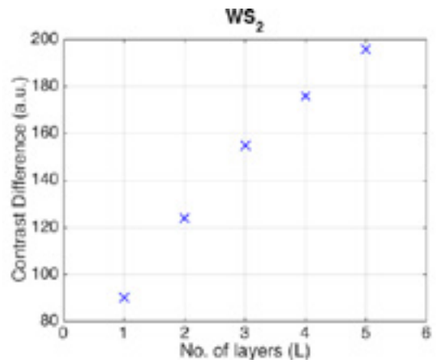

Figure 11 Contrast difference of blue light of few layer WS_2.

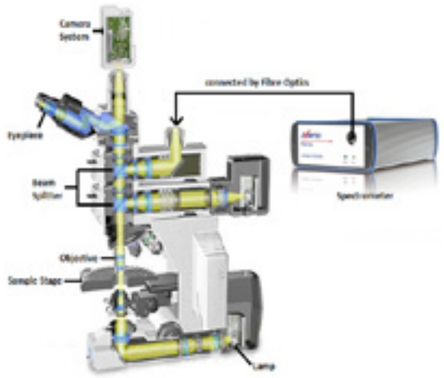

Figure 12 Schematics of microscope and spectrometer set up adapted from Nikon and Avantes.

fibre is then placed back on the spectrometer and tuned for maximum light detection. Before the actual transmission measurement, a dark spectrum I_{Dark} of detector counts in a range of wavelength is measured when the microscope lamp is switched off and no light is allowed to pass through to the camera and fiber optics. Dark noise is defined as the non-illuminated noise in Root Mean Square (RMS) for the shortest integration time, and the RMS is calculated over 100 scans. The dark spectrum typically looks like the graph in Figure 15. In subsequent measurements, the dark spectrum is always subtracted from the actual transmittance spectrum, in order to reduce dark noise.

When performing the actual transmission measurement, the bottom lamp

Figure 13 The red circle in the figure shows the detection area of the spectrometer, placed on the quartz background.

Figure 14 The red circle in the figure shows the detection area of the spectrometer, placed on a MoS_2 sample.

Optical transmittance measurement in vis-NIR

The optical transmission spectra are measured in ambient conditions using a micro- scope (Nikon Eclipse LV100D) with an attached spectrometer (AvaSpec-ULS2048L StarLine Versatile Fiber-optic Spectrometer). Figure 12 shows the schematic diagram of the spectrometer set up and Table 2 shows the specifications of the spectrometer. The spectrometer is able to measure in the UV-vis-NIR regime and through a circular detection area of ~2.5 µm radius. The exact detection area (out of the whole field of view) is determined by shining a flash light through the optical fibre of the spectrometer to the microscope, and then marking out the detection area of the spectrometer on the live image seen in the microscope software, NIS-Elements. The optical

Technical Data	
Optical Bench	ULS Symmetrical Czerny-Turner, 75 mm focal length
Wavelength range	200-1100 nm
Resolution	0.06-20 nm, depending on configuration
Stray-light	0.04-0.1%, depending on the grating
Sensitivity in counts/µW per ms integration time	470,000
Detector	CCD linear array, 2048 pixels
Signal/Noise	300:1
AD converter	16 bit, 2 MHz
Integration time	1.11 ms - 10 minutes
Interface	USB 2.0 high speed, 480 Mbps RS-232, 115,200 bps
Sample speed with on-board averaging	1.1 ms / scan
Data transfer speed	1.8 ms / scan (USB2) 430 ms / scan (RS-232)
Digital IO	HD-26 connector, 2 Analog in, 2 Analog out, 3 Digital in, 12 Digital out, trigger, sync.
Power supply	Default USB power, 350 mA or with SPU2 external 12VDC, 350 mA
Dimensions, weight	175 x 110 x 44 mm (1 channel), 716 grams

Table 2 Specifications of spectrometer adapted from Avantes.

of the microscope is switched on and the sample is placed in focus under the microscope. The sample has to be bigger than the detection area of the spectroscope so that the transmission spectrum is representative of a particular thickness of a material. A reference spectrum IRef of detector counts in a range of wavelength is taken when the detection area is placed somewhere around the sample where there is nothing else but quartz, and it typically looks like the graph in Figure 16. It is observed that the microscope lamp produces a significant number of counts in the region of 400 - 850 nm, which means that the detector would be sensitive to measurements done in that region. As such, the default region of interest is 400 - 850 nm.

This reference spectrum is set as 100% optical transmittance, which means that the reflectance and absorbance of quartz are taken into account and do not contribute to the measured spectra of the 2D crystals. This is so that the measured optical transmittance of any sample is with recpect to the light through quartz background. However, quartz itself has a certain value of transmittance and its optical transmission spectrum is measured as seen in Figure 17. In the visible light region, the average optical transmittance and absorbance are 88.6646% and 0.0523 respectively.

After proper calibration, the detection area is placed inside the sample to measure a spectrum I of detector counts in a range of wavelengths. The measurement steps are seen in Figure 13 and Figure 14. The optical transmittance T is then obtained in units of percentage (%) by using the relation:

$$T = (I - I_{Dark})/(I_{Ref} - I_{Dark})$$

After obtaining the transmission spectrum, the values can be converted to absorbance A, a unit-less quantity, following the Beer-Lambert law:

$$A = -\log_{10} T$$

This mathematical calculation neglects the reflectance of the sample which, in principle, can be measured using the top lamp on the microscope, but is outside the scope of this project.

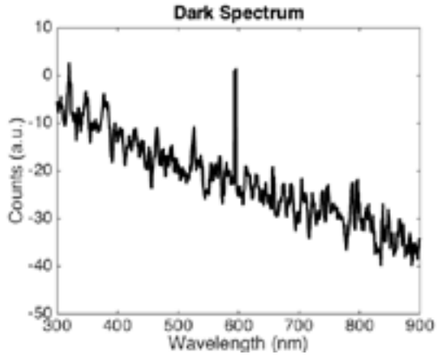

Figure 15 Detector counts spectrum of the dark spectrum.

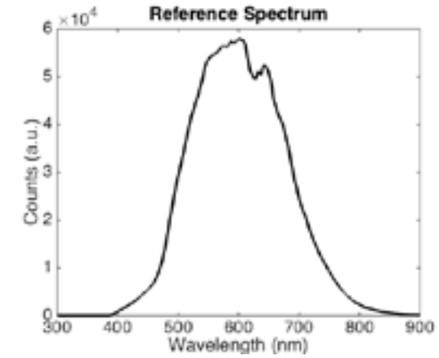

Figure 16 Detector counts spectrum of the reference spectrum.

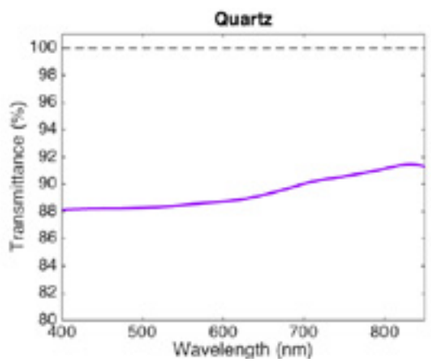

Figure 17 Typical transmission spectrum of the used quartz wafers.

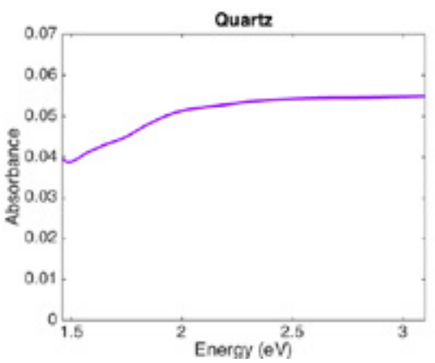

Figure 18 Typical absorbance spectrum of the used quartz wafers.

Results

In this chapter, the optical transmittance and absorbance of graphene, BN, several TMDs and their heterostructures, and bP are measured using the methods described in the “Optical transmittance measurement in” on page 12. A calibration of the experiment is done first to check the optimum light intensity settings and reproducibility of results, which are described in the first section. The following sections discuss the results of the different materials.

Calibration

In the spectroscopy experiment, the light intensity used on the microscope and reproducibility of results are checked to ensure that all parts of the spectroscopic measurements are accurate.

Figure 19 Optical images of bilayer MoS2 using Koehler illumination under low light intensity.

Figure 20 Optical images of bilayer MoS2 using Koehler illumination under medium light intensity.

Light Intensity

To find the optimum light intensity for the spectroscopy measurements, three different light intensities of the microscope lamp are tested to see their accuracy and stability of readings, as well as their accurate wavelength regions. This test mea- surement is done on a bilayer MoS2 sample. The optical images of the bilayer MoS2 sample under the different light intensities are seen in Figure 19, Figure 20, and Figure 21.

Figure 21 Optical images of bilayer MoS2 using Koehler illumination under high light intensity.

After performing the spectroscopic measurements, the transmission and absorbance spectra are obtained, as seen in Figure 22 and Figure 23. It is observed that with a higher light intensity, the transmittance and absorbance curves are smoother and have a wider range of wavelength accuracy. However, when the light intensity is too high, the B exciton peak is observed to saturate, whereby the transmittance (absorbance) increases (decreases). This is due to the non-linear optical effects at high light intensity, which can be explained by several mechanisms. The Pauli exclusion principle states that no two electrons are allowed to exist in the same state at the same place, so the probability of exciton creation would decrease when there is already a lot of excitons created. This results in saturation of the excition peak[41]. As such, the light intensity used in subsequent spectroscopic measuremnts is in the medium range.

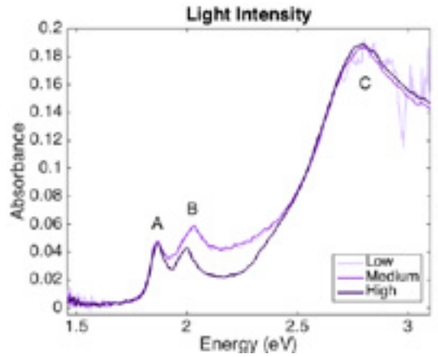

Figure 23 Absorbance spectrum of bilayer MoS_2 under different light intensities.

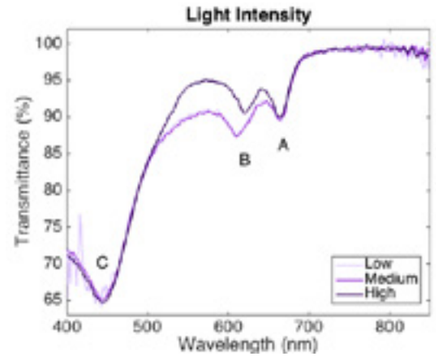

Figure 22 Transmission spectrum of bilayer MoS_2 under different light intensities.

Reproducibility

The reproducibility of results is checked by measuring different samples of bilayer MoS_2 to see if they produced the same curves with similar features. After verifying the layer number of the bilayer samples of MoS_2 using Raman spectroscopy as described in the subsection “Raman spectroscopy”, spectroscopic measurements of three samples are taken and the transmission and absorbance graphs obtained are seen in Figure 24 and Figure 25. It is observed that the curves overlap very well and the unique features of MoS_2 are retained in the curves. This shows the reproducibility of the spectroscopic measurement.

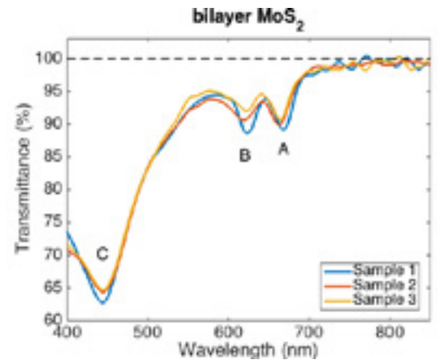

Figure 24 Transmission spectrum of three different samples of bilayer MoS_2.

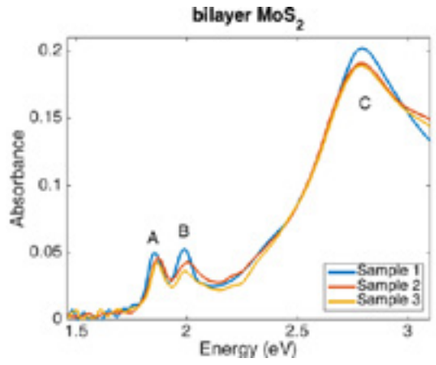

Figure 25 Absorbance spectrum of three different samples of bilayer MoS_2.

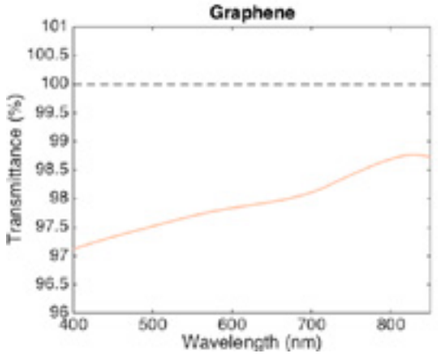

Figure 26 Transmission spectrum of graphene.

Graphene

The optical transmittance of graphene is measured and the transmission and ab- sorbance spectra are shown in Figure 26 and Figure 27. The transmission spectrum is observed to be almost uniform regardless of wavelength, and the average optical transmit- tance and absorbance in the visible light region (400 - 700 nm) is calculated to be 97.6332% and 0.0103 respectively. Comparing the optical transmittance with Nair[25], the value of optical transmittance of graphene is very similar with a percentage difference of 0.07%.

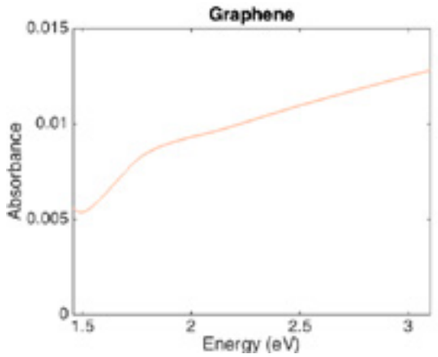

Figure 27 Absorbance spectrum of graphene.

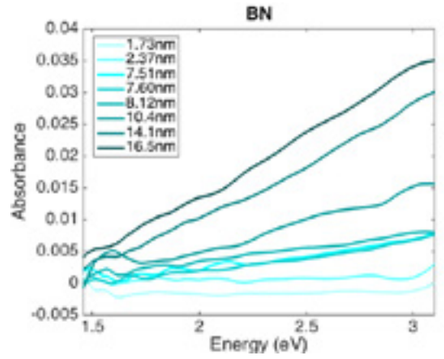

Figure 29 Absorbance spectrum of BN of thickness of 1.73 - 16.5 nm.

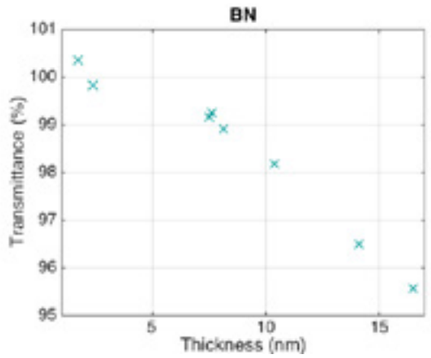

Figure 30 Graph of average transmittance of BN in the visible light range (400 - 700 nm) for thickness of 1.73 - 16.5 nm.

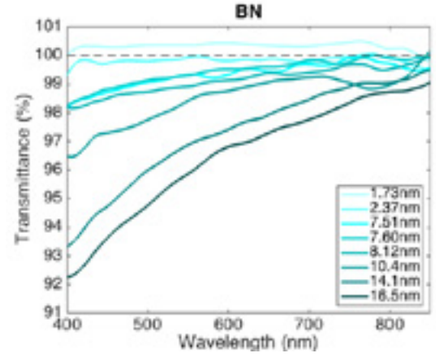

Figure 28 Transmission spectrum of BN of thickness of 1.73 - 16.5 nm.

Boron Nitride

The optical transmittance of BN of 1.73 - 16.5 nm thickness are also measured to obtain the transmission and absorbance spectrum, as seen in Figure 28 and Figure 29. The thickness of BN is measured with the AFM as described in the subsection “Atomic force microscopy”. BN is observed to transmit more red light than violet light, while the overall transmittance magnitude is higher for thinner BN crystals. BN of thickness less than 3 nm has almost 100% transmittance. Only at a thickness of about 8 nm, BN has a transmittance of 99%. The averaged optical transmittance and absorbance of the BN samples in the visible light region are plotted in Figure 30 and Figure 31.

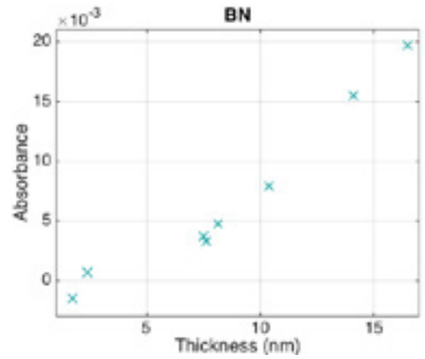

Figure 31 Graphs of average absorbance of BN in the visible light range (400 - 700 nm) for thickness of 1.73 - 16.5 nm.

Transition Metal Dichalcogenides

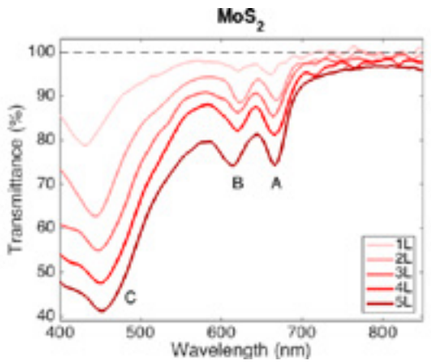

Figure 32 Transmission spectrum of 1 to 5 layers of MoS_2.

Molybdenum disulfide

The optical transmittance of MoS_2 of 1 to 5 layers have been measured and Figure 32 and Figure 33 shows the transmittance and absorbance spectra, respectively. The number of layers is de- termined using Raman spectroscopy as described in subsection “Raman spectroscopy”. It is observed that the overall transmittance (absorbance) magnitude is lower (higher) for increas- ing layer number of MoS_2. There are three peaks observed at about 440 nm, 620 nm, and 665nm in the transmittance spectrum (or 2.78 eV, 2.00 eV, and 1.86 eV in the absorbance spectrum) which corresponds to the C, B, and A excitonic transition peaks. It is deduced that violet, orange, and red light are least transmitted (or most absorbed) in MoS_2. This means that optically, few layer MoS_2 is seen to have hues of violet, orange and red, and it suggests that MoS_2 would be most easily seen with a violet, orange, or red filter. The averaged optical transmittance and absorbance of the MoS_2 samples in the visible light region are plotted in Figure 34 and Figure 35, respectively.

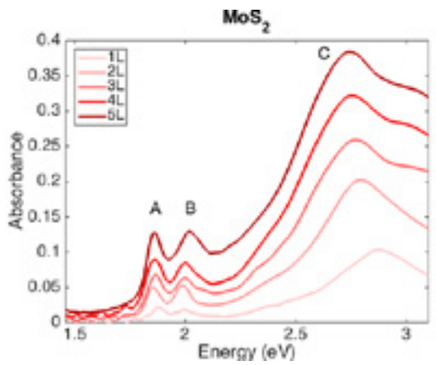

Figure 33 Absorbance spectrum of 1 to 5 layers of MoS_2.

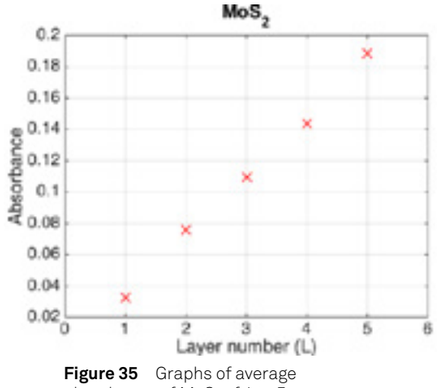

Figure 35 Graphs of average absorbance of MoS_2 of 1 to 5 layers in the visible light range (400 - 700 nm).

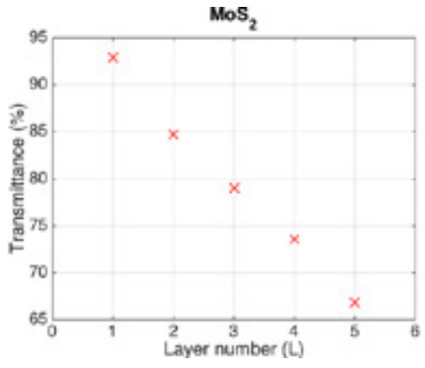

Figure 34 Graph of average transmittance of MoS_2 of 1 to 5 layers in the visible light range (400 - 700 nm).

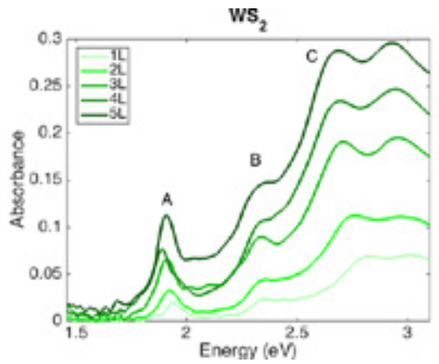

Figure 37 Absorbance spectrum of 1 to 5 layers of WS_2.

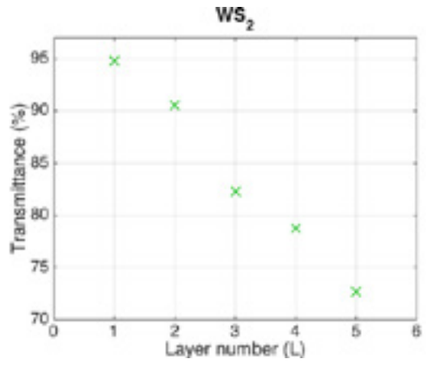

Figure 38 Graph of average transmittance of WS_2 of 1 to 5 layers in the visible light range (400 - 700 nm).

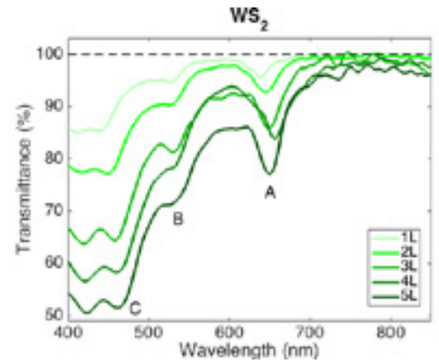

Figure 36 Transmission spectrum of 1 to 5 layers of WS_2.

Tungsten disulfide

Spectroscopic measurements are done on WS_2 and the transmission and absorbance spectra are shown in Figure 36 and Figure 37, repectively. The number of layers is determined using the methods described in the subsections “Photoluminescence Spectroscopy”, “Fluorescence Spectroscopy”, and “Optical Contrast”. It is observed that the overall transmittance (absorbance) magnitude is lower (higher) for increasing layer number of WS_2. There are three peaks observed at about 450 nm, 528 nm, and 648 nm in the transmittance spectrum (or 2.75 eV, 2.33 eV, and 1.91 eV in the absorbance spectrum) which corresponds to the C, B, and A excitonic transition peaks. It is deduced that blue, green, and red light are least transmitted (or most absorbed) in WS_2. This means that optically, few layer WS_2 is seen to have hues of blue, green and red, and again it suggests that MoS_2 would be most easily seen with a blue, green, or red filter. The averaged optical transmittance and absorbance of the WS_2 samples in the visible light region are plotted in Figure 38 and Figure 39, respectively.

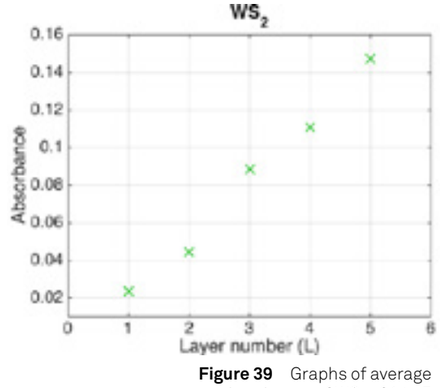

Figure 39 Graphs of average absorbance of WS_2 of 1 to 5 layers in the visible light range (400 - 700 nm).

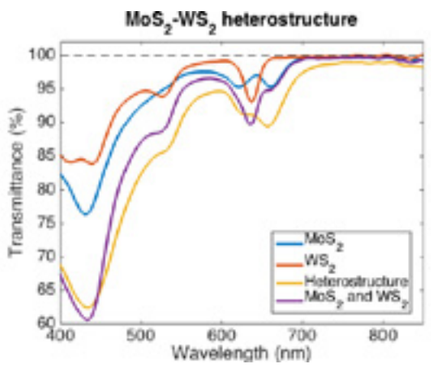

Figure 40 Transmission spectrum of MoS_2-WS_2 heterostructure and its components, as labelled in the legend.

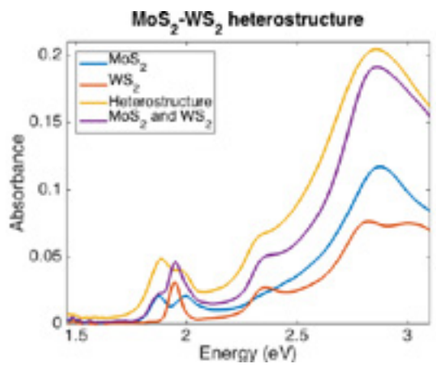

Figure 41 Absorbance spectrum of MoS_2-WS_2 heterostructure and its components, as labelled in the legend.

MoS_2-WS_2 heterostructure

The MoS_2-WS_2 heterostructure is made of a MoS_2 monolayer at the bottom and a WS_2 monolayer on top. The monolayer MoS_2 and WS_2 are identified using fluorescence spectroscopy in the subsection "Fluorescence Spectroscopy". The optical transmittance of the MoS_2-WS_2 heterostructure is measured to obtain the transmission and absorbance spectrum as seen in Figure 40 and Figure 41. Looking at the heterostructure transmission and absorbance curves, the A peak of WS_2 is overpowered by the A and B peaks of MoS_2 while both the C peaks combine to give an enhanced peak. The B peak of WS_2 is still distinct in the heterostructure curves. The combined transmittance and absorbance spectrum of the individual MoS_2 and WS_2 monolayers are also plotted in Figure 40 and Figure 41, depicted by the purple curve. The combined transmittance and absorbance of the individual layers does not differ much from that of the heterostructure, and there is only a slight shift in the A and B peaks of MoS_2. This is due to the band alignment of the heterostructure which will be explained further in the chapter "Discussion". The average optical transmittance and absorbance of the MoS_2-WS_2 heterostructure in the visible light region is calculated to be 84.0486% and 0.0797 respectively.

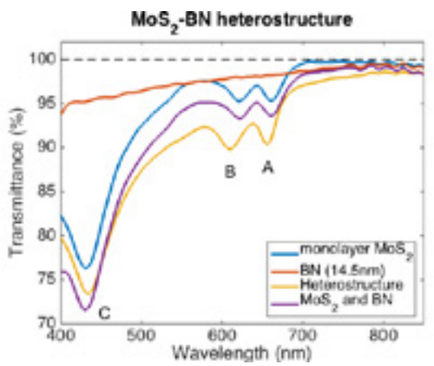

Figure 42 Transmission spectrum of MoS_2-BN heterostructure and its components, as labelled in the legend.

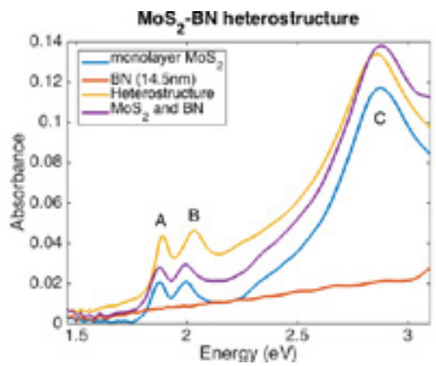

Figure 43 Absorbance spectrum of MoS_2-BN heterostructure and its components, as labelled in the legend.

MoS_2-BN heterostructure

The MoS_2-BN heterostructure is made of a MoS_2 monolayer at the bottom and a BN layer of 14.5 nm thickness on top. The monolayer MoS_2 is identified using fluorescence spectroscopy in the subsection "Fluorescence Spectroscopy", while the thickness of BN is measured with the AFM in the subsection "Atomic force microscopy". Spectroscopic measurements are also done on the MoS_2-BN heterostructure and the transmission and absorbance spectra in Figure 42 and Figure 43 are obtained. The transmission and absorbance curves of the heterostructure retains the features of MoS_2 and it suggests that BN does not impact the optical properties of the heterostructure much since its optical transmission curve is flat. This is proven by the combined transmittance and absorbance spectrum of the individual MoS_2 and BN layers, which are plotted in figure 4.12, depicted by the purple curve. The combined transmittance and absorbance spectrum is similar to that of the heterostructure, only that the heterostructure transmit (absorb) less (more) light around the A and B exciton peaks. The average optical transmittance and absorbance of the MoS_2-BN heterostructure in the visible light region is calculated to be 87.7273% and 0.0581 respectively.

Black Phosphorus

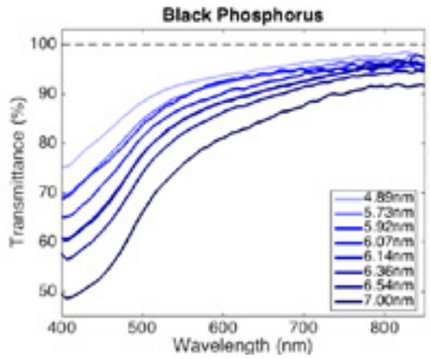

Figure 44 Transmission spectrum of bP with MgO encapsulation of thickness of 4.89 - 7.00 nm.

Optical Transmittance

To study the optical transmittance of bP, it has to be first encapsulated using MBE and dry transfer as described in section “Transfer”. Encapsulation is needed because bP is very reactive with air and oxidizes almost immediately upon exposure to air[42,43].

Firstly, bP crystals of 4.89 - 7.00 nm thickness that are capped with MgO are studied under the spectrometer. The thickness of the bP crystals is measured under the AFM as described in the subsection “Atomic force microscopy”. The transmission and absorbance spectra obtained are shown in Figure 44 and Figure 45. It is observed that bP generally transmits more red light than violet light, while the overall transmittance magnitude is higher for thinner bP crystals. The averaged optical transmittance and absorbance of the BN samples in the visible light region are plotted in figure 4.14. However, the bP samples are observed to oxidize even with the MgO encapsulation during the course of the experiment, albiet slower than without encapsulation. This was the stimulant for performing more optical transmittance measurements on bP but with graphene encapsulation instead.

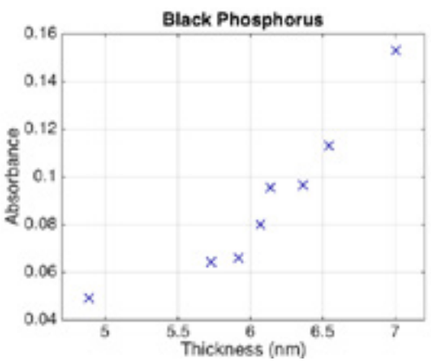

Figure 47 Graph of average absorbance of bP with MgO encapsulation in the visible light range (400 - 700 nm) for thickness of 4.89 - 7.00 nm.

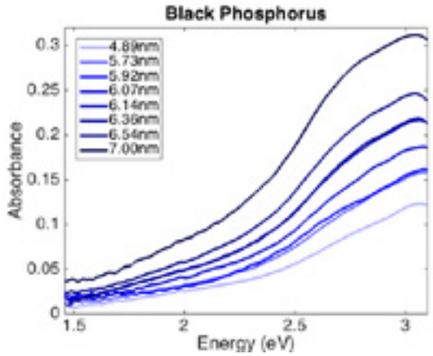

Figure 45 Absorbance spectrum of bP with MgO encapsulation of thickness of 4.89 - 7.00 nm.

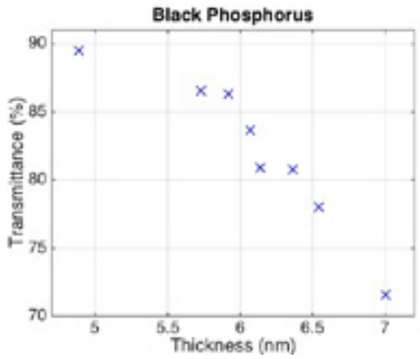

Figure 46 Graph of average transmittance of bP with MgO encapsulation in the visible light range (400 - 700 nm) for thickness of 4.89 - 7.00 nm.

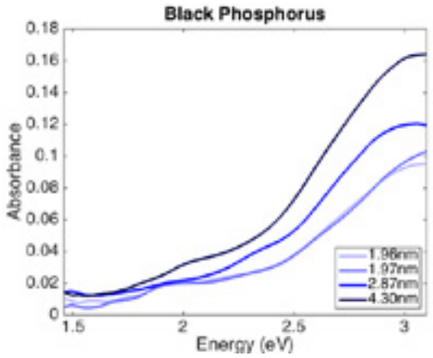

Figure 49 Absorbance spectrum of bP with graphene encapsulation of thickness of 1.96 - 4.30 nm.

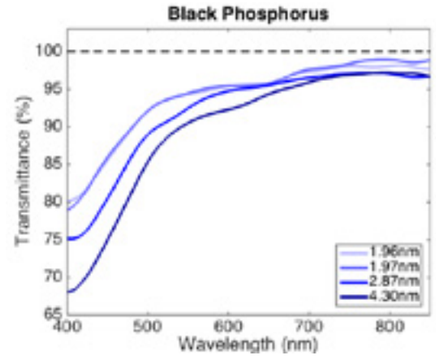

Figure 48 Transmission spectrum of bP with graphene encapsulation of thickness of 1.96 - 4.30 nm.

Next, bP crystals of 1.96 - 4.30 nm thickness that are capped with graphene are studied under the spectrometer. The thickness of the bP crystals is measured under the AFM as described in the subsection “Atomic force microscopy”. The transmission and absorbance spectra obtained are shown in Figure 48 and Figure 49. Again, it is observed that bP generally transmits more red light than violet light, while the overall transmittance magnitude is higher for thinner bP crystals. The averaged optical transmittance and absorbance of the bP samples in the visible light region are plotted in Figure 50 and Figure 51.

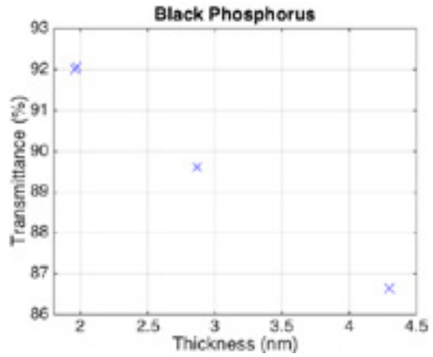

Figure 50 Graph of average transmittance of bP with graphene encapsulation in the visible light range (400 - 700 nm) for thickness of 1.96 - 4.30 nm.

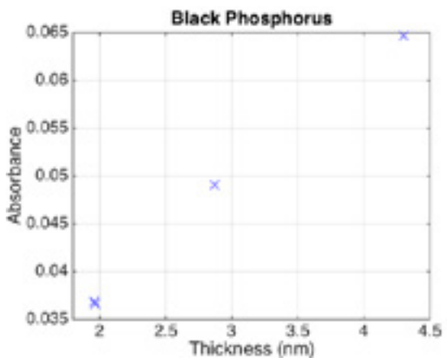

Figure 51 Graph of average absorbance of bP with graphene encapsulation in the visible light range (400 - 700 nm) for thickness of 1.96 - 4.30 nm.

Optical Anisotropy

To measure the dependence of the optical properties of bP on the angle of polarisation of light, a polariser is placed on top of the microscope lamp before it passes through the bP sample. Firstly, an arbitrary axis is defined to set the angle in which the polarizer should be placed. The optical image of a bP crystal of 1.96 nm thickness with graphene encapsulation oriented along the arbitrary axis is seen in Figure 53. The polarizer is then rotated in steps of 30° (from -90° to 90°) with respect to the arbitrary axis before taking the optical transmittance measurement.

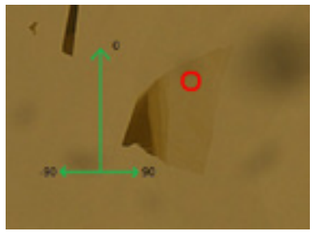

Figure 53 Optical image of bP crystal of 1.96 nm thickness with graphene encapsulation oriented along an arbitrary axis that is labelled with the green arrow on the left.

The transmission and absorbance spectra of the bP crystal of 1.96 nm thickness with graphene encapsulation oriented along the arbitrary axis is seen in Figure 52 and Figure 54. It is observed that the transmittance and absorbance changes at different angles, but only incident light at 433 nm or 2.85 eV is unaffected by the polarisation. At 0°, 15° and 30°, the bP crystal is observed to transmit (absorb) less (more) violet light and more (less) red to blue light in comparison to the curves of -30° and 60°, while it is the opposite at -90°, -60° and 90°.

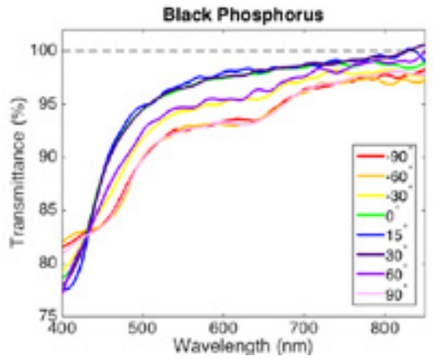

Figure 52 Transmission spectrum of bP of thickness of 1.96 nm with graphene encapsulation in which the polarizer is placed at -90° to 90° with respect to an arbitrary axis.

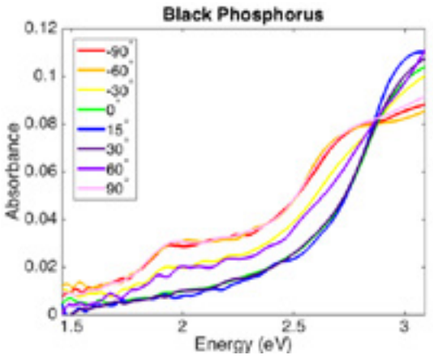

Figure 54 Absorbance spectrum of bP of thickness of 1.96 nm with graphene encapsulation in which the polarizer is placed at -90° to 90° with respect to an arbitrary axis.

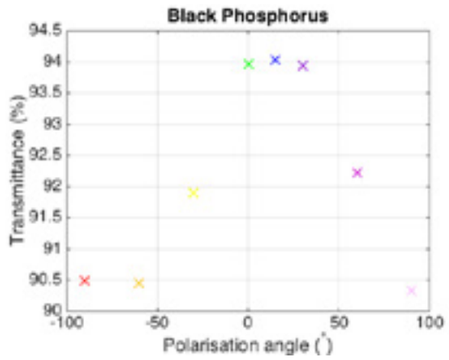

Figure 55 Graph of average transmittance of bP of thickness of 1.96 nm with graphene encapsulation in the visible light range (400 - 700 nm) in which the polarizer is placed at -90° to 90° with respect to an arbitrary axis.

The turning point for the change appears to be at 15°. This demonstrates the optical anisotropy of bP. The averaged optical transmittance and absorbance of the bP crystal in the visible light region when oriented at different angles along the arbitrary axis are plotted in Figure 55 and Figure 56. It is observed that at 15°, bP is transmits (absorbs) the most (least) incident light.

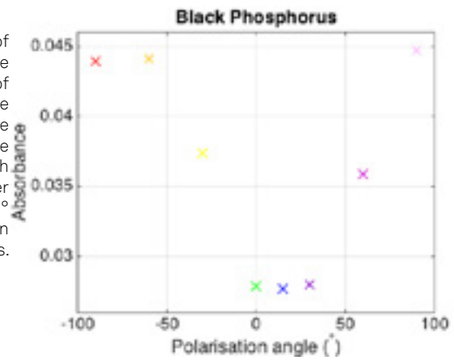

Figure 56 Graph of average transmittance of bP of thickness of 1.96 nm with graphene encapsulation in the visible light range (400 - 700 nm) in which the polarizer is placed at -90° to 90° with respect to an arbitrary axis.

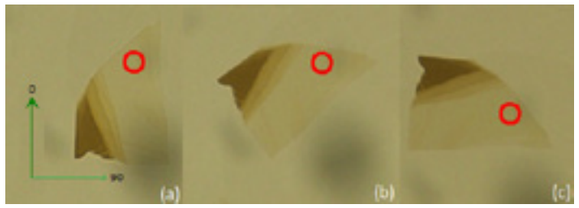

Figure 57 Optical image of bP crystal of 1.96 nm thickness with graphene encapsulation placed at (a) 0°, (b) 45°, and (c) 90° with respect to a polarizer whose direction is labeled with the green arrow on the left.

In order to confirm the anisotropy results, and exclude any potential polarization-dependence in the microscope's optical path, the experiment is repeated by keeping the polarizer fixed and rotating the sample. The bP crystal of 1.96 nm thickness with graphene encapsulation is measured under the spectrometer when the sample is placed at 0°, 45°, and 90° with respect to the polarizer, as seen in Figure 57.

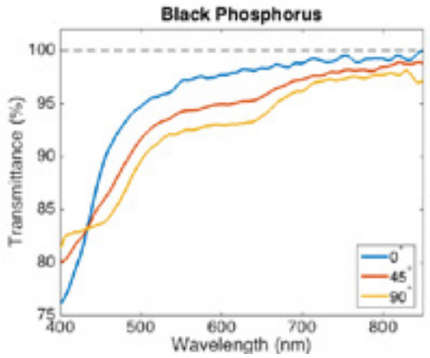

Figure 58 Transmission spectrum of bP of thickness of 1.96 nm with graphene encapsulation that is placed at 0 to 90° with respect to the direction of a polarizer.

Angle (·)	Transmittance (%)	Absorbance
0	94.0261	0.0278
45	91.8346	0.0377
90	90.3707	0.0445

Table 3 Table of various thickness of bP with graphene encapsulation of thickness of 1.96 nm that is placed at 0 to 90° with respect to a polarizer, and the corresponding average optical transmittance and absorbance in the visible light region (400 - 700 nm) at each angle.

The transmission and absorbance graphs of the bP crystal of 1.96 nm thickness are seen in Figure 58 and Figure 59. Again, it is observed that the transmittance and absorbance changes at different angles, but only light at 433 nm or 2.85 eV are unaffected by the polarisation. At 0° the bP crystal is observed to transmit (absorb) less (more) violet light and more (less) red to blue light in comparison to the curve of 45°, while it is the opposite at 90°. The average optical transmittance and absorbance of bP in the visible light region are calculated in Table 3. It is observed that when polarised at 0° with respect to a polarizer, bP would transmit the most visible light, which means it is optically more transparent.

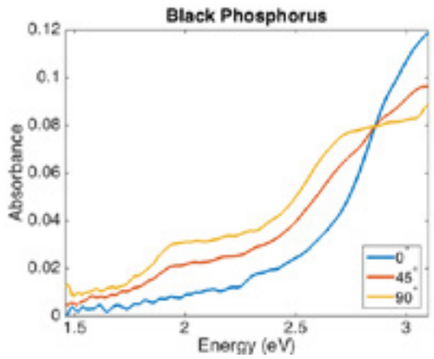

Figure 59 Absorbance spectrum of bP of thickness of 1.96 nm with graphene encapsulation that is placed at 0 to 90° with respect to the direction of a polarizer.

Figure 60 Optical image of bP crystal of 2.87 nm thickness with graphene encapsulation placed at (a) 0°, (b) 45°, and (c) 90° with respect to a polarizer whose direction is labeled with the green arrow on the left.

Finally, the previous measurement is done again on a bP flake with a different thickness to check if the exepriment is reproducible. A bP crystal of 2.87 nm thickness with graphene encapsulation is measured under the spectrometer when the sample is placed at 0°, 45°, and 90° with respect to the polarizer, as seen in Figure 60.

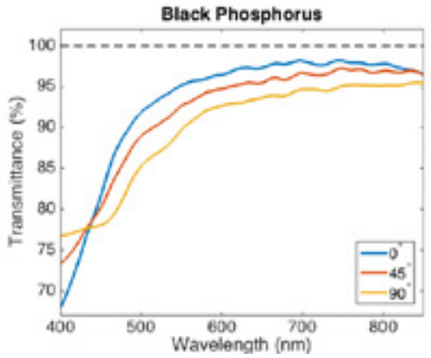

Figure 61 Transmission spectrum of bP of thickness of 2.87 nm with graphene encapsulation that is placed at 0 to 90° with respect to the direction of a polarizer.

Angle (.)	Transmittance (%)	Absorbance
0	91.2227	0.0419
45	89.6380	0.0489
90	87.5301	0.0590

Table 4 Table of various thickness of bP with graphene encapsulation of thickness of 2.87 nm that is placed at 0 to 90° with respect to a polarizer, and the corresponding average optical transmittance and absorbance in the visible light region (400 - 700 nm) at each angle.

The transmission and absorbance graphs of the bP crystal of 2.87 nm thickness are seen in Figure 61 and Figure 62. Indeed, the anisotropy measurement is reproducible since the results are similar to the previous experiment. The averaged optical transmittance and absorbance of bP in the visible light region (400 - 700 nm) are calculated in Table 4.

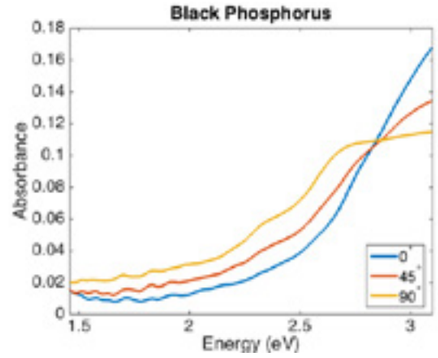

Figure 62 Absorbance spectrum of bP of thickness of 2.87 nm with graphene encapsulation that is placed at 0 to 90° with respect to the direction of a polarizer.

Discussion

This chapter explains the characteristics of the measured optical transmittance and absorbance presented in the chapter 4.

Graphene

In the optical transmittance measurements of graphene presented in Figure 26, it is observed that the averaged transmittance is 97.7377% and almost constant across the measured wavelength region. This independence can be explained by dimensional analysis since the Hamiltonian of graphene which describes the linear bands has no intrinsic energy scale to compare with the photon energy. The calculation of the absorption in perturbation theory directly shows the independence, since the ω and v_F dependence are cancelled by three important parameters: the square of the transition matrix element ($\propto v_F^2/\omega^2$), the joint density of states ($\propto \omega/v_F^2$), and the photon energy ($\propto \omega$). Their product defines the optical absorption[44]. However, there is a slight deviation in transmittance and absorbance in the blue light region (400 - 500 nm, or 2.5 -3.1 eV) which is due to surface contaminants. Hydrocarbon contamination is a highly plausible reason as the dry transfer process as described in the section "Transfer", which uses polymers (PMMA and PMGI), is known to leave residue on the transferred sample and substrate. These polymers used are known to absord light in the blue light to UV light range, hence producing the deviation in the optical transmittance measurement of graphene. In Nair's work on the optical transmittance of graphene, a similar effect is seen as well[25].

Boron Nitride

The optical transmittance measurements of BN presented in Figure 28 show that BN has a high optical transparency compared to other 2D crystals of similat thickness. This is due to its large band gap of ~6.5 eV[12]. The energy of visible light is not enough to excite the electrons from the valence band to the conduction band, since visible light has photon energy in the range of 1.8 eV to 3.1 eV. As such, visible light passes through without being absorbed, which makes the appearance of BN transparent. Also, excitonic effects are not observed in the visible light spectrum because of the large band gap. Wirtz, Marini, and Rubio[45] presented the absorption spectra of bulk and monolayer BN in the range of 4 eV to 8.5 eV. The study shows an excitonic peak in the absorption spectra at ~6 eV. The spectrum also broadens out beyond the peak, which explains the gentle slope of the measured absorbance spectrum of BN in Figure 29.

Transition Metal Dichalcogenides

The measured transmittance and absorbance of MoS_2 and WS_2 in Figure 32, Figure 33, Figure 36 and Figure 37 respectively, show the high visibility of these materials in comparison with the other 2D crystals of similar thickness. This is becuse thin layers of MoS_2 and WS_2 have band gap energies in the visible light region, so they absorb visible light. The transmittance and absorbance spectra contain three well defined exciton peaks, labelled as A, B, and C, from low to high energies.

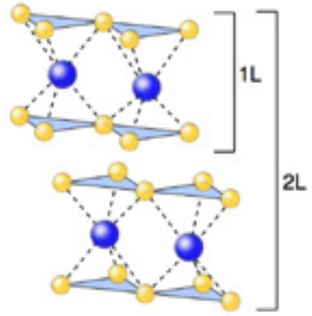

Figure 63 Lattice structures of monolayer and bilayer MX_2, obtained from ref 46.

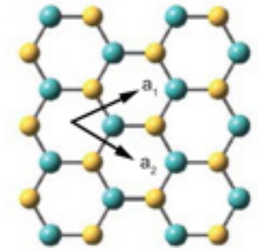

Figure 64 Schematic illustration of the structure of monolayer MX_2 where the blue and yellow spheres represent metal and chalcogen atoms respectively Schematic illustration of the structure of monolayer MX_2 where the blue and yellow spheres represent metal and chalcogen atoms respectively. Obtained from ref 29.

For MoS_2, the A, B and C peaks occur at 440 nm, 620 nm, and 665nm (or 2.78 eV, 2.00 eV, and 1.86 eV), respectively. For WS_2, the A, B and C peaks occur at 450 nm, 528 nm, and 648 nm (or 2.75 eV, 2.33 eV, and 1.91 eV), respectively. These features are attributed to excitonic effects, which are understood with the crystal and band structures of the TMDs. The crystal structure of TMDs shown in Figure 63, Figure 64 and Figure 65 comprises of layers of strongly bonded X-M-X atoms that are held together by weak van der Waals forces, where each layer of M and X atoms forms a 2D hexagonal crystal.

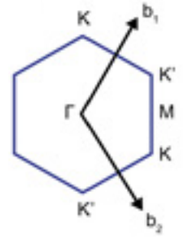

Figure 65 First Brillouin zone of monolayer MX_2, obtained from ref 29.

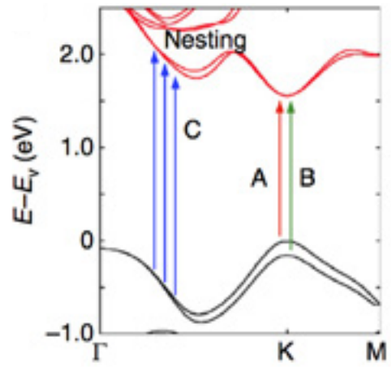

Figure 66 The band structure of monolayer MoS_2 with the transition in A, B and C, indicated by the arrows. Obtained from ref 46.

Since the group 6 MX_2 are isoelectronic, the features of the electronic structure are generally identical. The conduction band minimum and the valence band maximum are both located at the *K/K'* point of the Brillouin zone for monolayer MX_2. When moving from the direct to indirect band gap, the transition between the conduction band valley at the **Λ** point and the valence band hill at the **Γ** point becomes prominent. For the MoS_2 and WS_2 monolayers, band-nesting effects occurs in the middle of the **Λ** and **Γ** points. The exciton A and B peaks correspond to the transition from the spin-orbit split valence bands to the lowest conduction band at the *K* and *K'* points, while the C peak is related to the transition from the valence band to the conduction band between the **Λ** and **Γ** point of the Brillouin zone, as seen in Figure 66.

The strong absorption at high energies, which is the C peak for MoS_2 and WS_2, is due to the nearly-degenerate exciton states. This feature is represented by the region of the Brillouin zone where the valence and conduction bands are nested, under the single-electron band structure picture. The band structure in Figure 66 also depicts the energy required for the A, B, and C excitonic transitions, which explains their position in the measured transmittance and absorbance spectra.

Heterostructures

In the optical transmittance measurements of the MoS_2-WS_2 heterostructure presented in Figure 40 and Figure 41, the heterostructure spectrum retains the A and B peaks of MoS_2, and the B peak of WS_2, while the C peaks of both materials combine to give an enhanced peak. Comparing with the combined transmittance and absorbance spectrum of the individual MoS_2 and WS_2 monolayers, the shape is similar, only that the heterostructure transmit (absorb) less (more) light around the A and B exciton peaks. This is understood by the combined band structure of the MoS_2-WS_2 heterostructure.

The MoS_2-WS_2 heterostructure forms a type II alignment since the states around the *K* point are localized to one of the monolayers. The valence band maximum and the conduction band minimum are localised to the WS2 and the MoS2 monolayers repectively, as seen in Figure 67. At the **Γ**-point, the mixing of the bands are due to the interaction between the MoS_2 and WS_2 monolayers which results in a strong shift or splitting of the energy levels. As a result, the band gap becomes indirect because the valence-band **Γ**-point states are pushed 0.15 eV higher than the *K*-point states[47]. However, the theoretical calculation of the optical absorption spectrum of the MoS_2-WS_2 heterostructure does not show the indirect transitions as direct transitions at the *K*-point dominate[5, 34,48]. The optically active transitions are composed of direct intralayer transitions, while the interlayer transitions were found with intensities close to zero. As such, the optical properties are very weakly affected by the interlayer interactions and the distinct optical properties of the TMD layers are mostly retained in the heterostructure. This explains the weak shift in transmittance and absorbance at the A and B exciton peaks, and high similarity of the overall shapes of the combined optical transmittance and absorbance spectra MoS_2 and WS_2 monolayers and that of their heterostructure, as seen in Figure 40 and Figure 41.

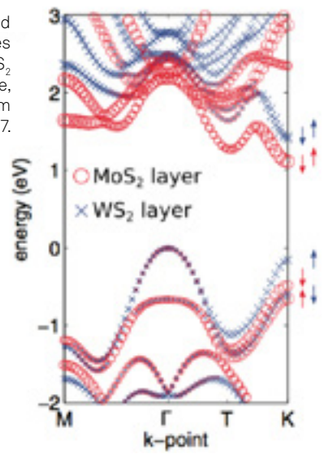

Figure 67 Band structures of MoS_2-WS_2 heterostructure, obtained from ref 47.

For the MoS_2-BN heterostructure, the distinct optical properties of each material are retained in the transmittance and absorbance spectrum of the heterostructure as presented in Figure 42 and Figure 43. This is suggested by the high similarity between the combined transmittance and absorbance spectrum of the individual MoS_2 and WS_2 layers and that of the heterostructure. This is because of the almost negligible interaction between the two layers. Looking at the band structure, the BN layer does not affect the **Γ**-point band edge of MoS_2. They have a type I alignment as seen in Figure 68, since the valence band maximum of BN at the K point is below that of MoS_2 and the conduction band minimum at the K point is above that of MoS_2[47]. Since there is very little interaction at the band edge of the MoS_2 and BN layers, this explains the optical transmittance and absorbance spectra of the the MoS_2-BN heterostructure, which is similar to the combined spectra of each layer, as seen in Figure 42 and Figure 43.

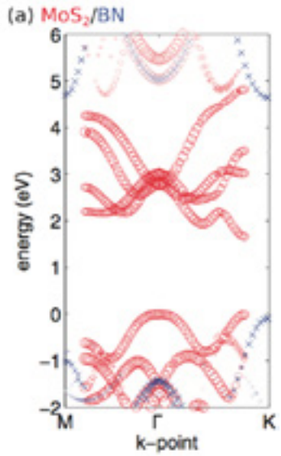

Figure 68 Band structures of MoS_2-BN heterostructure, obtained from ref 47.

Black Phosphorus

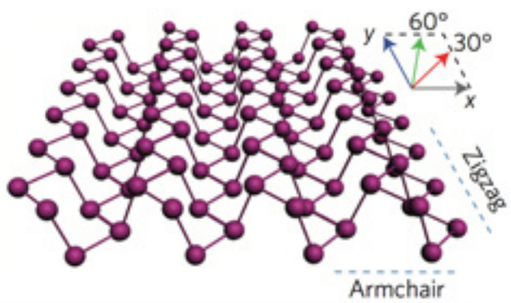

Figure 69 Schematic structural view of phosphorene and its crystal orientation, obtained from ref 20.

Optical Anisotropy

The different transmittance and absorbance spectra of bP with light polarised in different directions, as seen in the results of the section “Optical Anisotropy”, is explained by the crystal and band structure of phosphorene. The crystal structure of phosphorene is seen in Figure 69, where each phosphorus atom in black phosphorus is covalently bonded to three adjacent atoms that forms a puckered honeycomb network. The x-axis is the armchair direction, while the y-axis is the zigzag direction. In comparison with the band structure in k-space as seen in Figure 70, the **Γ**-Y direction and the **Γ**-X direction correspond to the armchair and the zigzag direction respectively. It is observed that both top of valence bands and the bottom of conduction bands have much more significant dispersions along the **Γ**-Y direction, but are nearly flat along the **Γ**-X direction[24]. This shows its highly anisotropic band dispersion around the band gap at the **Γ** point. Based on previous experimental and theoretical works[49,50], the transitions between the conduction band valleys and valence band hills are allowed for light polarized along the armchair direction, but it is partially allowed for light polarized along the zigzag direction. Tran, Soklaski, Liang, and Yang[17] also demostrated theoretically that absorption of light polarised in the armchair direction is higher than that of light polarised in the zigzag direction.

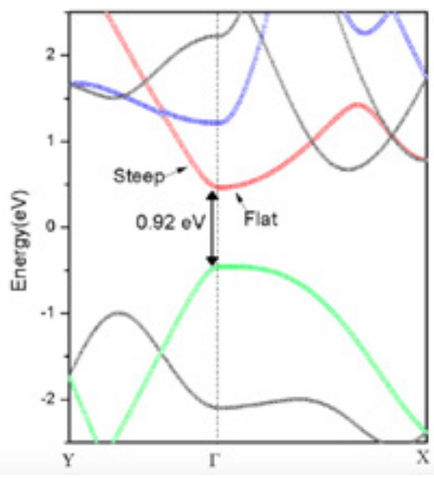

Figure 70 Band structure of phosphorene, where the direct band gap of 0.92 eV is located at the **Γ** point, as obtained from ref 24.

Optical Transmittance

The optical transmittance measurements of bP with MgO and graphene presented in Figure 44 and Figure 48 respectively shows that bP is a very transparent material compared to the other studied 2D materials of similar thickness, second to BN. This is because its band gap is in the infrared (0.0012 - 1.65 eV) to red light region, which is 0.3 eV in the bulk form and 2 eV in the single layer form of phosphorene[17,18]. Visible light would provide more than enough energy to excite the electrons across the band gap. Since the required energy is less than that of visible light, its optical properties are not highly visible and looks highly transparent to the naked eye. The steep slope at the blue light region (400 nm or 3.1 eV) is speculated to be the tail of the excitonic effects that is expected in UV light region. It is noted that excitonic effects are observed in the absorption spectrum of bP[17,20], but there is no conclusive value of the exciton binding energy of bP since it could vary with different light polarisation.

In the results in Figure 52, Figure 54, Figure 55 and Figure 56, it is observed that a bP sample of 1.96 nm thickness with graphene encapsulation has different transmittance and absorbance spectra with different light polarisation. In particular, it has the highest (lowest) visible light transmittance (absorbance) at 15° from the arbitrary axis labelled in Figure 53. Applying the above information, it can be deduced that 15° from the arbitrary axis is the zigzag direction of the crystal structure of bP since the bP sample absorbs the least visible light at the angle. This means that the zigzag direction is the flat edge along the thinnest part of the bP sample, which is the part of lowest opacity. On the other hand, -75° from the arbitrary axis is inferred as the armchair direction of the crystal structure of bP since the bP sample absorbs the most visible light at the angle. The exact crystal axis of the bP sample can be determined by Raman spectroscopy, which is not included in the scope of this project due to time constraints.

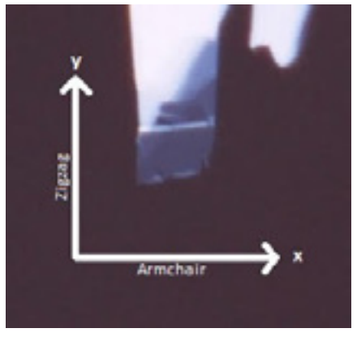

Figure 72 Optical image of bP crystal of 2.86 nm thickness with graphene encapsulation with its crystal axis labelled.

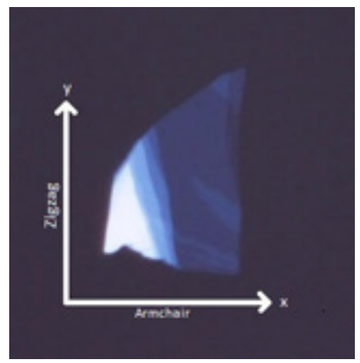

Figure 71 Optical image of bP crystal of 1.96 nm thickness with graphene encapsulation with its crystal axis labelled.

The zigzag and armchair direction of the bP sample of 1.96 nm thickness with graphene encapsulation is confirmed by the results of Figure 58, Figure 59, and Table 3. The visible light absorbance is the weakest when the flat edge along the thinnest part of the bP sample is oriented in the same direction as the incident light polarisation. This suggests that the direction along the flat edge is the zigzag direction of the bP crystal, while the perpendicular edge is the armchair direction. This is depicted in Figure 71.

The same experimental method is applied to a bP sample of thickness of 2.87 nm with graphene encapsulation and its measured transmittance is in Figure 61, Figure 62, and Table 4. The optical anisotropy of bP is observed when the measured transmittancevaries when the crystal is oriented at different directions with respect to the incident light polaristion. Since the absorbance of visible light is lowest at 0° while highest at 90°, it is deduced that the crystal edge that is in the same direction with the incident light polaristion at 0° is the zigzag direction. The crystal edge perpendicular to that previously mentioned is along the armchair direction. The directions along the crystal are depicted in Figure 72.

Conclusion & Outlook

In summary, the optical transmittance of exfoliated 2D crystals and their heterostructures was experimentally measured, and it was observed to be thickness dependent. Among the 2D crystals of similar thickness, boron nitride is the most transparent while molebdenum disulfide is the most opaque. The optical transmit- tance of the materials are can be explained by the respective band structure and energy gap; the material would appear more opaque if the band gap is in or near the visible light range (400 - 700 nm). The optical transmittance of the studied heterostructures exhibits the optical transmittance properties of the individual layers of the heterostructures since there is little interaction between them. Only the optical transmittance of graphene is independent of the photon excitation energy, while the rest of the materials are have excitonic effects. The optical transmittance of black phosphorus is seen to be tunable by ~3.7% when adjusting the light po- larisation along the crystal axis. This is attributed to the anisotropy of the crystal structure of black phosphorus. These results show the potential for using these 2D materials in transparent electronics, with the light polarisation control of the optical transmittance of black phosphorus as an extra degree of freedom.

In the course of this experiment, hydrocarbon contamination might have caused the optical transmittance to deviate from the intrinsic value due to the use of polymers in the dry transfer method. To produce pristine samples for proper optical study, further research in transfer methods is required. Besides sample purity, additional measurements could be taken to complete the current findings. The crystal axis of black phosphorus should be determined with Raman spectroscopy to provide complete information on the optical anisotropy of black phosphorus. Another example is the reflectance measurements of the studied 2D crystals which would complement our existing data. It enables us to fully characterise the optical properties of the studied 2D materials by obtaining the dielectric function. However, reflectance in thin layers of 2D materials are minimal since the atomically thin materials are more transmissive than reflective. Reflectance measurement is usually done on bulk materials since they intrinsically reflect more light and are opaque. This is the driving factor for this project to focus on optical transmittance measurement.

There are many possibilities to extend this research in the future, and one of them is to study the electric field tunability of the optical transmittance of the 2D materials. Since the optical transmittance is seen to be tied so closely with the electronic properties of 2D materials, this future study would provide further insights on the connection between these properties. The effect of electric-field gating could be used to gain further insights on the suitability of the materials in the application of transparent devices. Next, a study of the strain effects on the optical properties of the 2D materials could also be done in the future. By combining the new information on the mechanical properties of the 2D materials with the measured optical and electronic properties, this opens a pathway to build next generation transparent flexible electronics.

ACKNOWLEDGEMENTS

I would like express my gratitude towards to Prof. Barbaros Özyilmaz and Rostislav Aleksandrov Doganov for the great feedback and guidance throughout the research project. Also, I would like to thank my colleagues who taught me all the experimental skills for making this project possible and my research experience an enjoyable one.

Biblography

1. K. S. Novoselov, A. K. Geim, S. Morozov, D Jiang, Y. Zhang, S. Dubonos, I. Grigorieva, and A. Firsov, "*Electric field effect in atomically thin carbon films*," Science, vol. 306, no. 5696, pp. 666–669, 2004.

2. K. Novoselov, S. Morozov, T. Mohinddin, L. Ponomarenko, D. Elias, R Yang, I. Barbolina, P Blake, T. Booth, D Jiang, et al., "*Electronic properties of graphene*," Physica status solidi (b), vol. 244, no. 11, pp. 4106–4111, 2007.

3. S. D. Sarma, S. Adam, E. Hwang, and E. Rossi, "*Electronic transport in two-dimensional graphene*," Reviews of Modern Physics, vol. 83, no. 2, p. 407, 2011.

4. A. Splendiani, L. Sun, Y. Zhang, T. Li, J. Kim, C.-Y. Chim, G. Galli, and F. Wang, "*Emerging photoluminescence in monolayer MoS_2*," Nano letters, vol. 10, no. 4, pp. 1271–1275, 2010.

5. K. F. Mak, C. Lee, J. Hone, J. Shan, and T. F. Heinz, "*Atomically thin MoS_2: A new direct-gap semiconductor*," Physical Review Letters, vol. 105, no. 13, p. 136 805, 2010.

6. Z. G. Yu, Y. Cai, and Y.-W. Zhang, "*Robust direct band-gap characteristics of one- and two-dimensional ReS_2*," Scientific reports, vol. 5, 2015.

7. I. G. Lezama, A. Arora, A. Ubaldini, C. Barreteau, E. Giannini, M. Potemski, and A. F. Morpurgo, "*Indirect-to-direct band gap crossover in few-layer $MoTe_2$*," Nano letters, vol. 15, no. 4, pp. 2336–2342, 2015.

8. G. D. Scholes and G. Rumbles, "*Excitons in nanoscale systems*," Nature materials, vol. 5, no. 9, pp. 683–696, 2006.

9. Y. Yu, Y. Yu, Y. Cai, W. Li, A. Gurarslan, H. Peelaers, D. E. Aspnes, C. G. Van de Walle, N. V. Nguyen, Y.-W. Zhang, et al., "*Exciton-dominated dielectric function of atomically thin MoS_2 films,*" Scientific reports, vol. 5, 2015.

10. R. Neville and B. Evans, "*The band edge excitons in 2H-MoS_2*," Physica status solidi (b), vol. 73, no. 2, pp. 597–606, 1976.

11. K. I. Bolotin, K. Sikes, Z. Jiang, M Klima, G Fudenberg, J Hone, P. Kim, and H. Stormer, "*Ultrahigh electron mobility in suspended graphene*," Solid State Communications, vol. 146, no. 9, pp. 351–355, 2008.

12. X. Du, J Li, J. Lin, and H. Jiang, "*The origins of near band-edge transitions in hexagonal boron nitride epilayers*," Applied Physics Letters, vol. 108, no. 5, p. 052 106, 2016.

13. A. Kuc, N. Zibouche, and T. Heine, "*Influence of quantum confinement on the electronic structure of the transition metal sulfide TS_2*," Physical Review B, vol. 83, no. 24, p. 245 213, 2011.

14. L. Li, Y. Yu, G.J. Ye, Q. Ge, X. Ou, H. Wu, D. Feng, X.H. Chen, and Y. Zhang, "*Black phosphorus field-effect transistors*," Nature nanotechnology, vol. 9, no. 5, pp. 372–377, 2014.

15. M. Buscema, D. J. Groenendijk, S. I. Blanter, G. A. Steele, H. S. van der Zant, and A. Castellanos-Gomez, "*Fast and broadband photoresponse of few-layer black phosphorus field-effect transistors,*" Nano letters, vol. 14, no. 6, pp. 3347–3352, 2014.

16. H. Liu, A. T. Neal, Z. Zhu, Z. Luo, X. Xu, D. Tománek, and P. D. Ye, "*Phosphorene: An unexplored 2d semiconductor with a high hole mobility*," ACS nano, vol. 8, no. 4, pp. 4033–4041, 2014.

17. V. Tran, R. Soklaski, Y. Liang, and L. Yang, "*Layer-controlled band gap and anisotropic excitons in few-layer black phosphorus*," Physical Review B, vol. 89, no. 23, p. 235 319, 2014.

18. S. Fukuoka, T. Taen, and T. Osada, "*Electronic structure and the properties of phosphorene systems*," ArXiv preprint arXiv:1507.00703, 2015.

19. N. Mao, J. Tang, L. Xie, J. Wu, B. Han, J. Lin, S. Deng, W. Ji, H. Xu, K. Liu, et al., "*Optical anisotropy of black phosphorus in the visible regime*," Journal of the American Chemical Society, 2015.

20. X. Wang, A. M. Jones, K. L. Seyler, V. Tran, Y. Jia, H. Zhao, H. Wang, L. Yang, X. Xu, and F. Xia, "*Highly anisotropic and robust excitons in monolayer black phosphorus*," Nature nanotechnology, vol. 10, no. 6, pp. 517–521, 2015.

21. A. Rodin, A Carvalho, and A. C. Neto, "*Strain-induced gap modification in black phosphorus*," Physical review letters, vol. 112, no. 17, p. 176 801, 2014.

22. T. Hong, B. Chamlagain, W. Lin, H.-J. Chuang, M. Pan, Z. Zhou, and Y.-Q. Xu, "*Polarized photocurrent response in black phosphorus field-effect transistors*," Nanoscale, vol. 6, no. 15, pp. 8978–8983, 2014.

23. J. Qiao, X. Kong, Z.-X. Hu, F. Yang, and W. Ji, "*High-mobility transport anisotropy and linear dichroism in few-layer black phosphorus*," Nature communications, vol. 5, 2014.

24. R. Fei and L. Yang, "*Strain-engineering the anisotropic electrical conductance of few-layer black phosphorus*," Nano letters, vol. 14, no. 5, pp. 2884–2889, 2014.

25. R. Nair, P Blake, A. Grigorenko, K. Novoselov, T. Booth, T Stauber, N. Peres, and A. Geim, "*Fine structure constant defines visual transparency of graphene*," Science, vol. 320, no. 5881, pp. 1308–1308, 2008.

26. L. Falkovsky, "*Optical properties of graphene*," in Journal of Physics: Conference Series, IOP Publishing, vol. 129, 2008, p. 012 004.

27. A. Zunger, A. Katzir, and A. Halperin, "*Optical properties of hexagonal boron nitride*," Physical Review B, vol. 13, no. 12, p. 5560, 1976.

28. L. Song, L. Ci, H. Lu, P. B. Sorokin, C. Jin, J. Ni, A. G. Kvashnin, D. G. Kvashnin, J. Lou, B. I. Yakobson, et al., "*Large scale growth and characterization of atomic hexagonal boron nitride layers*," Nano letters, vol. 10, no. 8, pp. 3209–3215, 2010.

29. R. Kumar, I. Verzhbitskiy, and G. Eda, "*Strong optical absorption and photocarrier relaxation in 2-d semiconductors*," Quantum Electronics, IEEE Journal of, vol. 51, no. 10, pp. 1–6, 2015.

30. Y. Li, A. Chernikov, X. Zhang, A. Rigosi, H. M. Hill, A. M. van der Zande, D. A. Chenet, E.-M. Shih, J. Hone, and T. F. Heinz, "*Measurement of the optical dielectric function of monolayer transition-metal dichalcogenides: MoS_2, $MoSe_2$, WS_2, and WSe_2*," Physical Review B, vol. 90, no. 20, p. 205 422, 2014.

31. A. Castellanos-Gomez, L. Vicarelli, E. Prada, J. O. Island, K. Narasimha-Acharya, S. I. Blanter, D. J. Groenendijk, M. Buscema, G. A. Steele, J. Alvarez, et al., "*Isolation and characterization of few-layer black phosphorus*," 2D Materials, vol. 1, no. 2, p. 025 001, 2014.

32. T. Low, A. Rodin, A Carvalho, Y. Jiang, H. Wang, F. Xia, and A. C. Neto, "*Tunable optical properties of multilayer black phosphorus thin films*," Physical Review B, vol. 90, no. 7, p. 075 434, 2014.

33. A. Avsar, J. Y. Tan, T Taychatanapat, J Balakrishnan, G. Koon, Y Yeo, J Lahiri, A Carvalho, A. Rodin, E. O'Farrell, et al., "*Spin–orbit proximity effect in graphene*," Nature communications, vol. 5, 2014.

34. W. Zhao, Z. Ghorannevis, L. Chu, M. Toh, C. Kloc, P.-H. Tan, and G. Eda, "*Evolution of electronic structure in atomically thin sheets of WS_2 and WSe_2*," ACS nano, vol. 7, no. 1, pp. 791–797, 2012.

35. T. Taniguchi and K. Watanabe, "*Synthesis of high-purity boron nitride single crystals under high pressure by using Ba-BN solvent*," Journal of crystal growth, vol. 303, no. 2, pp. 525–529, 2007.

36. J. Tan, A Avsar, J Balakrishnan, G. Koon, T Taychatanapat, E. O'Farrell, K Watanabe, T Taniguchi, G Eda, A. C. Neto, et al., "*Electronic transport in graphene-based heterostructures*," Applied Physics Letters, vol. 104, no. 18, p. 183 504, 2014.

37. R. A. Doganov, E. C. O'Farrell, S. P. Koenig, Y. Yeo, A. Ziletti, A. Carvalho, D. K. Campbell, D. F. Coker, K. Watanabe, T. Taniguchi, et al., "*Transport properties of pristine few-layer black phosphorus by van der waals passivation in an inert atmosphere*," Nature communications, vol. 6, 2015.

38. A. Ferrari, J. Meyer, V Scardaci, C Casiraghi, M. Lazzeri, F. Mauri, S Piscanec, D. Jiang, K. Novoselov, S Roth, et al., "*Raman spectrum of graphene and graphene layers*," Physical review letters, vol. 97, no. 18, p. 187 401, 2006.

39. A. Molina-Sanchez and L. Wirtz, "*Phonons in single-layer and few-layer MoS_2 and WS_2*," Physical Review B, vol. 84, no. 15, p. 155413, 2011.

40. H. Li, J. Wu, X. Huang, G. Lu, J. Yang, X. Lu, Q. Xiong, and H. Zhang, "*Rapid and reliable thickness identification of two-dimensional nanosheets using optical microscopy,*" ACS nano, vol. 7, no. 11, pp. 10 344–10 353, 2013.

41. D. A. Miller, "*Optical physics of quantum wells*," Quantum Dynamics of Simple Systems, 1st ed. G.-L. Oppo, SM Barnett, E. Riis, and M. Wilkinson (Institute of Physics, London, 1996), pp. 239–26, 1996.

42. J. O. Island, G. A. Steele, H. S. van der Zant, and A. Castellanos-Gomez, "*Environmental instability of few-layer black phosphorus*," 2D Materials, vol. 2, no. 1, p. 011 002, 2015.

43. S. P. Koenig, R. A. Doganov, H. Schmidt, A. C. Neto, and B. Oezyilmaz, "*Electric field effect in ultrathin black phosphorus*," Applied Physics Letters, vol. 104, no. 10, p. 103 106, 2014.

44. K. F. Mak, L. Ju, F. Wang, and T. F. Heinz, "*Optical spectroscopy of graphene: From the far infrared to the ultraviolet*," Solid State Communications, vol. 152, no. 15, pp. 1341–1349, 2012.

45. L. Wirtz, A. Marini, and A. Rubio, "*Excitons in boron nitride nanotubes: Dimensionality effects*," Physical review letters, vol. 96, no. 12, p. 126104, 2006.

46. D. Kozawa, R. Kumar, A. Carvalho, K. K. Amara, W. Zhao, S. Wang, M. Toh, R. M. Ribeiro, A. C. Neto, K. Matsuda, et al., "*Photocarrier relaxation pathway in two-dimensional semiconducting transition metal dichalcogenides*," Nature communications, vol. 5, 2014.

47. H.-P. Komsa and A. V. Krasheninnikov, "*Electronic structures and optical properties of realistic transition metal dichalcogenide heterostructures from first principles*," Physical Review B, vol. 88, no. 8, p. 085 318, 2013.

48. H.-P. Komsa and A. V. Krasheninnikov, "*Effects of confinement and environment on the electronic structure and exciton binding energy of MoS_2 from first principles*," Physical Review B, vol. 86, no. 24, p. 241 201, 2012.

49. A, Morita, "*Semiconducting black phosphorus*," Applied Physics A, vol. 39, no. 4, pp. 227–242, 1986.

50. Y. Akahama, S. Endo, and S.-i. Narita, "*Electrical properties of black phosphorus single crystals*," Journal of the Physical Society of Japan, vol. 52, no. 6, pp. 2148–2155, 1983.